Discover Oncology

Analysis

Development and validation of a prognostic risk score model for hepatocellular carcinoma in the Asian population based on immunogenic cell death-related genes

Zhengyang Feng[1,2] · Yanjie Wang[1] · Yong Liang[3] · Xuhao Gu[4] · Yinyin Yang[4] · Yusong Zhang[1] · Qiliang Peng[4]

Received: 26 June 2024 / Accepted: 25 November 2024
Published online: 04 December 2024

Abstract

Background Hepatocellular carcinoma (HCC), the predominant form of liver cancer, is marked by limited therapeutic success and unfavorable prognoses. Its etiology varies regionally, with hepatitis B virus (HBV) being the predominant cause in most of Asia. Immunogenic cell death (ICD), a specific type of cell death, has been extensively linked to HCC treatment in numerous studies. This research aims to explore the significance of ICD-related genes in the Asian HCC cohort, potentially offering novel approaches for HCC management.

Methods We initially obtained transcriptomic and clinical data pertinent to Asian HCC from the TCGA database. Subsequently, we classified the samples into distinct subgroups according to ICD gene expression levels and conducted analyses of the tumor microenvironment and enrichment. Furthermore, we randomly allocated the samples into training and testing cohorts, thereafter developing and validating an ICD gene-based prognostic model tailored for the Asian HCC population.

Results The Asian HCC samples were categorized into two subgroups: high and low ICD expression. In the low ICD expression group, we observed diminished infiltration of immune and stromal cells, increased tumor purity, and improved prognosis. Moreover, we devised a 5-gene risk-score prognostic model comprising BAX, CASP8, HMGB1, HSP90AA1, and IL6, demonstrating efficacy in prognostic predictions for the Asian HCC cohort.

Conclusion Our investigation unveils new perspectives on the influence of ICDs within Asian HCC populations. The derived 5-gene risk-score prognostic model, based on ICDs, not only serves as a tool for assessing prognosis in Asian HCC cases but also suggests potential therapeutic targets for HCC treatment.

Keywords Immunogenic cell death · Hepatocellular carcinoma · Tumor microenvironment · Prognostic model · Asian population

Zhengyang Feng, Yanjie Wang and Yong Liang contributed equally to this work and share first authorship.

Supplementary Information The online version contains supplementary material available at https://doi.org/10.1007/s12672-024-01630-9.

✉ Yusong Zhang, zhangyusong19@163.com; ✉ Qiliang Peng, pengqiliang1912@163.com; Zhengyang Feng, fengzhengyang92@163.com; Yanjie Wang, wwyanjie@163.com; Yong Liang, liangyong-777@163.com; Xuhao Gu, gxh501063@163.com; Yinyin Yang, yangyin33@yeah.net | [1]Department of Oncology, The Second Affiliated Hospital of Soochow University, Suzhou, China. [2]State Key Laboratory of Radiation Medicine and Protection, Soochow University, Suzhou, China. [3]Department of Oncology, The Fifth People's Hospital of Huai'an, Huai'an, China. [4]Department of Radiotherapy & Oncology, The Second Affiliated Hospital of Soochow University, Suzhou, China.

1 Introduction

Liver cancer ranks as the seventh most prevalent cancer globally, with the second highest mortality rate among cancer-related deaths [1]. Hepatocellular carcinoma (HCC) constitutes approximately 90% of liver cancer cases. The incidence and mortality of HCC are notably high in East Asia and Africa, and it is anticipated to become the third leading cause of cancer-related deaths by 2030 [2]. The etiology of HCC varies by region, with hepatitis B virus (HBV) being the primary cause in most of Asia (excluding Japan), South America, and Africa. Conversely, hepatitis C virus (HCV) predominates in Western Europe, North America, and Japan, while in Central and Eastern Europe, alcohol consumption is the main factor [3, 4]. HCC is notoriously resistant to therapy and generally prognosticates poor outcomes. The immune system plays a crucial role in both the development and treatment of HCC. In recent years, immunotherapies such as PD-1, PD-L1, CTLA4 inhibitors, along with CAR-T and TCR-T cells, have emerged as promising treatments for HCC. Based on immune cell infiltration, HCC can be categorized into various subtypes-immune-active, immune-exhausted, immune-intermediate, and immune-excluded [5]. About 20% of cases, termed immune-active HCC, feature substantial infiltrations of active helper (CD4+) and cytotoxic (CD8+) T cells, showing responsiveness to ICIs. In contrast, immune-excluded tumors typically exhibit inherent resistance to ICIs [6]. Enhancing immune cell infiltration in the tumor microenvironment is posited as a potent strategy to augment HCC immunotherapy outcomes.

Immunogenic cell death (ICD) is a cell death mechanism that provokes an immune response by releasing tumor-associated (TAA) and tumor-specific antigens (TSA). ICD is largely driven by damage-associated molecular patterns (DAMPs), including surface calreticulin (CRT), secreted ATP, and released high mobility group protein B1 (HMGB1) [7]. Specific cytotoxic chemotherapies (e.g., mitoxantrone, oxaliplatin, vincristine) and physiotherapies (radiation, photodynamic therapy) induce ICD in tumor cells, transforming them from non-immunogenic to immunogenic. This transition recruits and activates immune cells, thereby stimulating or enhancing anti-tumor immunity. Studies demonstrate that an increase in T lymphocytes and a higher ratio of cytotoxic CD8+ T cells over FOXP3+ regulatory T cells (Tregs) post-chemotherapy are indicative of favorable responses in breast and colorectal cancer patients treated with anthracyclines and oxaliplatin, respectively [8–10].

ICD-related biomarkers were notably elevated post-treatment of human and murine HCC cells with oxaliplatin, thereby illustrating oxaliplatin's dual role as both an ICD inducer and a tumor immune microenvironment modulator [11]. Icaritin elicited mitophagy and apoptosis, inciting ICD in both mouse Hepa1-6 and human Huh7 HCC cells. The icaritin and doxorubicin combination not only reshaped the immunosuppressive tumor microenvironment but also incited a potent immune memory response, significantly enhancing anti-HCC efficacy in early-stage mouse HCC models [12]. This indicates that anticancer therapies may transcend traditional cell elimination, potentially engaging ICD-related biomarkers to stimulate antitumor immunity and modify the tumor microenvironment in HCC patients.

These promising discoveries have sparked a wave of ICD-focused research. However, the scarcity of reliable and precise ICD biomarkers for HCC necessitates further exploration. Given the regional etiological variations and East Asia's high HCC incidence, we focused on the Asian population. This study aims to identify ICD-related biomarkers in Asian HCC patients and investigate their potential pathogenic roles in HCC. It is essential to develop an ICD risk-score model to evaluate prognosis, examine the immune microenvironment, and guide clinical treatment strategies for Asian HCC patients.

2 Materials and methods

2.1 Data acquisition

The workflow of this study is depicted in Fig. 1. We sourced transcriptome sequencing data, clinical details, and gene mutation information of 161 Asian HCC patients from the TCGA-LIHC project, accessed in October 2022 via the TCGA website (https://portal.gdc.cancer.gov/). Detailed clinical information is presented in Table 1.

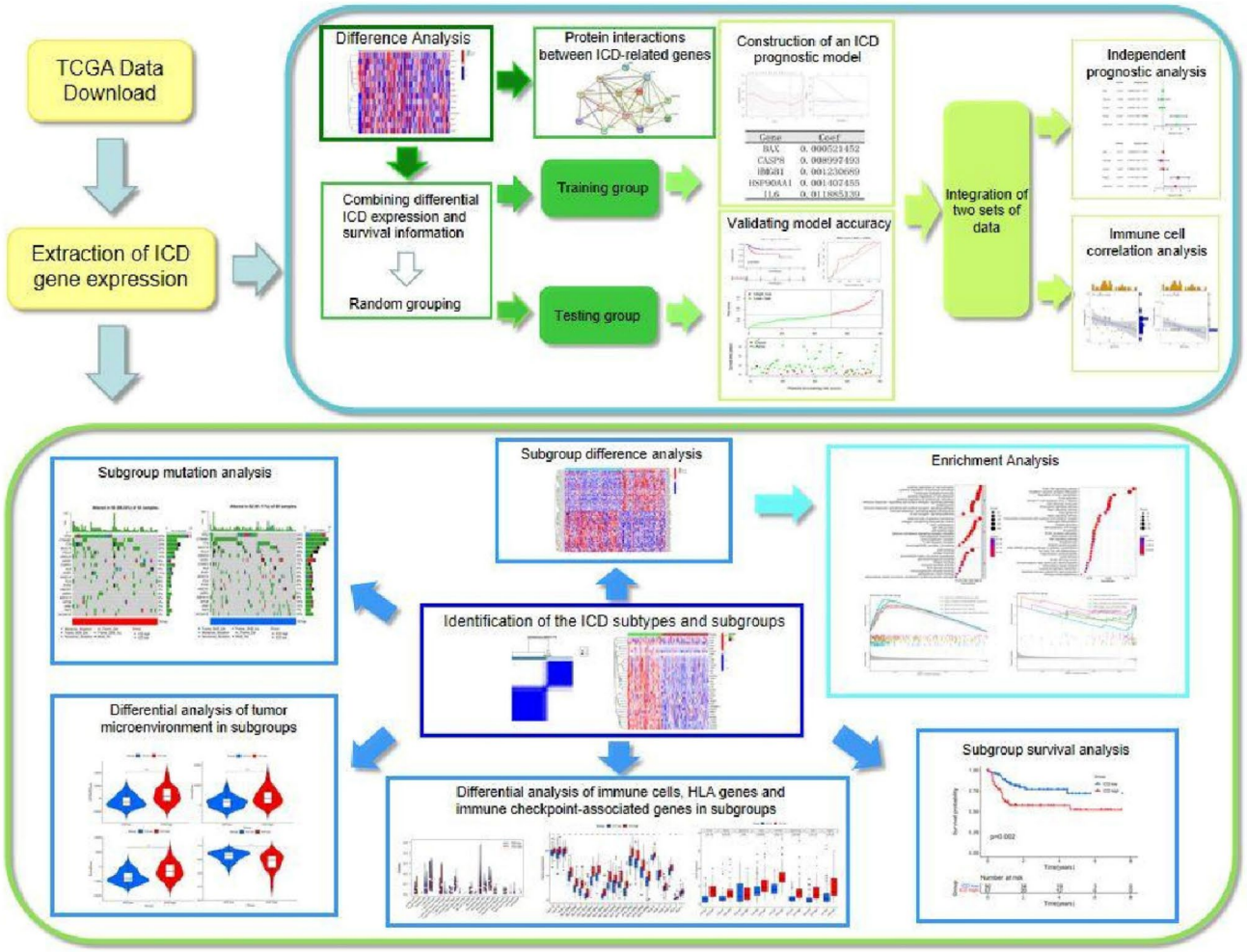

Fig. 1 Workflow of this study

2.2 Extraction of ICD gene expression

From prior research, we identified 143 ICD-related genes from previous studies (Table S1) [13–18]. We then extracted their expression data from the TCGA transcriptome information.

2.3 Construction of protein–protein interaction (PPI) network

Differential gene analysis was conducted using the "WilcoxTest" function in R. The criteria for filtering included: FDR ≤ 0.05 (FDR value represents the false discovery rate), $|\log_2 FC| \geq 1$ ($\log_2 FC = \frac{Mean\ value\ of\ gene\ expression\ in\ tumor\ samples}{Mean\ value\ of\ gene\ expression\ in\ normal\ samples}$), so as to filter out the ICD related genes with differences. Subsequently, we utilized the STRING database for PPI network analysis, aiming to establish connections between these ICD related gene nodes.

2.4 Identification of ICD subgroups

We classified the samples into distinct subtypes based on the expression of ICD-related genes, utilizing the "ConsensusClusterPlus" package in R. To ensure the stability of the results, we conducted ten replicates, each sampling 80% of the samples, guided by the area under the consensus cumulative distribution curve, k-values, and intragroup

Table 1 Clinical features of 161 Asian HCC patients

Clinical feature	Classification	Number	Proportion (%)
Age	≤65	125	77.64
	>65	35	21.74
	Unknown	1	0.62
Gender	Female	34	21.12
	Male	127	78.88
Grade	G1	14	8.70
	G2	64	39.75
	G3	71	44.10
	G4	12	7.45
Stage	I	81	50.31
	II	36	22.36
	III	41	25.47
	IV	1	0.62
	Unknown	2	1.24
TNM			
T	T1	82	50.93
	T2	36	22.36
	T3	37	22.98
	T4	6	3.73
N	N0	149	92.55
	N1	1	0.62
	NX	11	6.83
M	M0	153	95.03
	M1	1	0.62
	MX	7	4.35
Survival state	Survival	117	72.67
	Dead	44	27.33

consistency. Subsequently, the subtypes were categorized into two groups: ICD high expression group and ICD low expression group, based on the ICD gene expression.

2.5 Comparison of ICD subgroups

Kaplan–Meier (K–M) survival curves were generated using the "ggsurvplot" function in R, facilitating the comparison of survival rates between the ICD high and low expression groups. Differential analysis was conducted using the "wilcoxTest" in R, aiming to identify ICD-related genes with significant variation between these groups.

To further elucidate the significance of these differential genes, we undertook GO, KEGG, and GSEA enrichment analyses. Somatic mutation data for the SKCM samples were procured from TCGA GDC Data Portal in "maf" format, and a chi-squared test was employed to assess variations in gene mutation frequency across the sample groups.

We applied the estimate package in R to calculate scores for tumor cells, stromal cells, and immune cells, as well as tumor purity in each sample. This was followed by a differential analysis of the tumor microenvironment between subgroups using the "ggpubr" package, aiming to discern disparities in the tumor microenvironment between the high and low ICD expression groups.

The CIBERSORT algorithm facilitated the determination of immune cell content in each sample. We then utilized the "limma" package for analyzing differences in immune cells across subgroups, thus assessing the variation of each immune cell type between the high and low ICD expression groups.

Finally, differential analysis of HLA genes and common immune checkpoint-associated genes across subgroups was executed using the "limma" package to determine if notable differences existed between the high and low ICD expression groups.

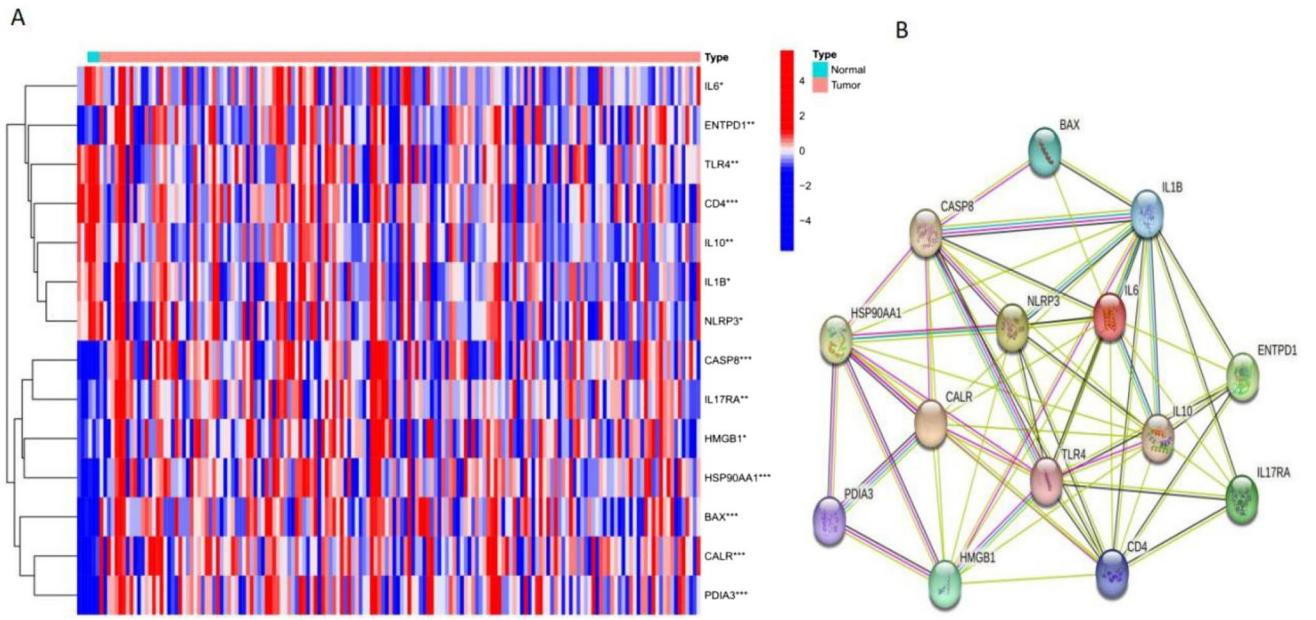

Fig. 2 Differential expression of 14 ICD-related genes. **A** Heat map illustrating the expression levels of 14 ICD-related genes. The horizontal axis represents sample names (blue for normal samples, red for tumor samples), and the vertical axis lists the names of differential ICD related genes. Genes marked with an asterisk indicate significant differences between normal and tumor samples. Significance levels are denoted as follows: ***p-value < 0.001, **p-value < 0.01, *p-value < 0.05. Blue signifies low expression, white indicates intermediate expression, and red denotes high expression. **B** PPI network among the 14 differential ICD-related genes

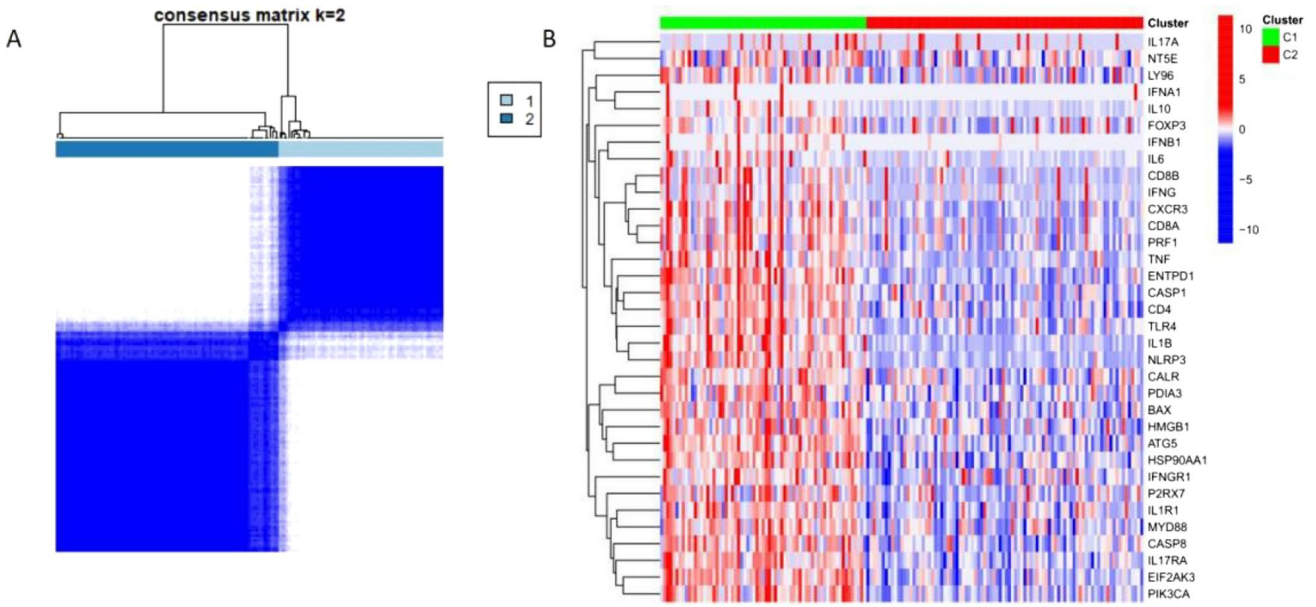

Fig. 3 Subgroup classification of Asian HCC samples based on ICD-related genes. **A** Heat map showing the consensus clustering result (k = 2) for 34 ICD-related genes in 161 Asian HCC samples. **B** Heat map displaying the expression of 34 ICD-related genes in C1 and C2 subtypes. The horizontal axis represents sample names, with the front green section indicating C1 subtype samples and the rear red section representing C2 subtype samples. The vertical axis displays the expression levels of ICD-related genes. Color coding for expression levels is as follows: blue for low expression, white for intermediate expression, and red for high expression

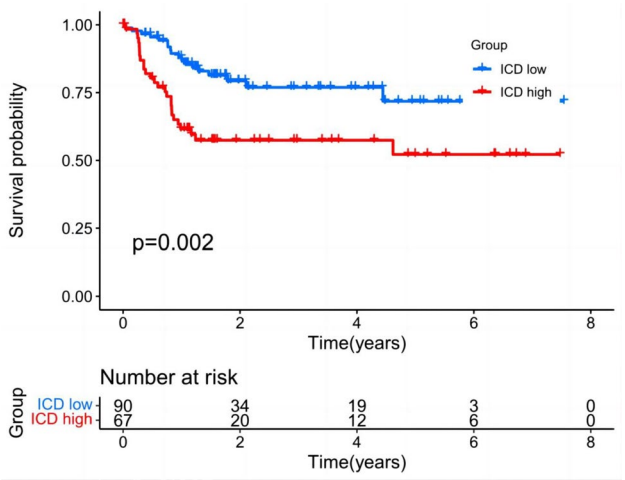

Fig. 4 Kaplan–Meier (K–M) survival curves for ICD high and low expression groups. This figure presents the survival curves, with the horizontal axis indicating survival time in years and the vertical axis showing the survival rate, which diminishes over time. The blue curve represents the low ICD expression group, while the red curve denotes the high ICD expression group

2.6 Construction and validation of the ICD prognostic model

The Asian HCC dataset, obtained from the TCGA database, was randomly segregated into two groups using the caret package in R: a training group for model construction and a testing group for validation. We combined survival time, survival status, and gene expression data using the "glmnet" package and conducted regression analysis via Lasso–Cox. Additionally, we implemented a tenfold cross-validation to ascertain the optimal model. Subsequently, K–M survival curves, ROC curves, and risk curves were plotted for both training and testing groups to verify the model's accuracy. Further analyses included univariate and multifactorial independent prognostic assessments, along with immune cell correlation analysis.

2.7 Clinical correlation analysis

All clinical features obtained from the TCGA database were divided into two groups as follows: age: ≤ 65 and > 65 years, sex: male and female, pathological grade: G1–2 and G3–4, pathological stage: stages I–II and stages III–IV, T stage: T1–2 and T3–4, M stage: M0 and 1 (cases with distant metastases), and N stage: N0 and 1 (cases with lymph node metastasis). The risk score, were compared with each clinical trait and analyzed for correlation by using the "beeswarm" package in R. A P-value less than 0.05 indicated that the genes or risk score was associated with a specific clinical characteristic.

2.8 Statistical analysis

All data were analyzed using R version 4.2.1. "WilcoxTest" was employed for differential analysis, and Fisher's exact test was used for enrichment analysis of differential genes. The risk model was developed through univariate Cox and LASSO regression analysis. K–M survival curves and ROC curves were utilized to evaluate the model's accuracy. A P-value < 0.05 was deemed statistically significant.

3 Results

3.1 PPI network between ICD related gene nodes

The differential analysis identified 14 ICD-related genes with significant variations between normal and tumor samples (Fig. 2A), including CD4, CASP8, HSP90AA1, BAX, CALR, and PDIA3, all exhibiting highly significant differences (P-values < 0.001); ENTPD1, TLR4, IL10, and IL17RA showed notable differences (P-values < 0.01); while IL6, IL1B, NLRP3,

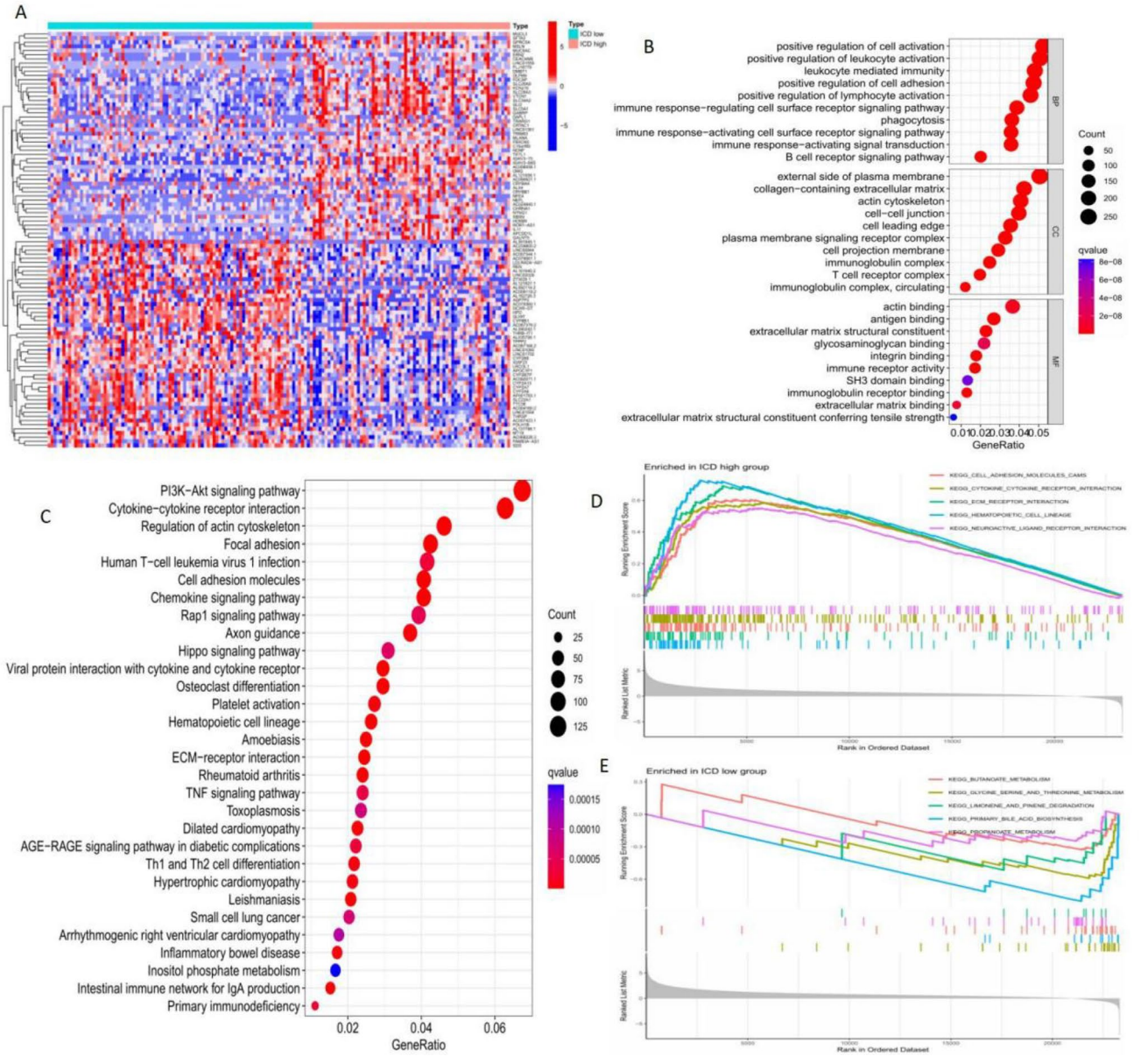

Fig. 5 Enrichment analysis of differential genes between ICD high and low expression groups. **A** Heat map illustrating the differential gene expression in ICD high and low expression groups. **B** Bubble chart of GO enrichment analysis for differential genes. The horizontal axis shows the gene ratio, and the vertical axis lists the GO categories: Biological Process (BP), Cell Component (CC), and Molecular Function (MF). The circle size indicates the number of genes; larger circles represent greater gene enrichment in GO, and a redder hue indicates higher enrichment levels. **C** Bubble chart of KEGG enrichment analysis for differential genes. The horizontal axis displays the gene ratio, and the vertical axis shows KEGG pathways. As with GO, circle size denotes the number of genes, and a redder color signifies higher enrichment. **D** GSEA enrichment results for the ICD high expression group. **E** GSEA results for the ICD low expression group. The horizontal axis represents the sequenced genes, and the vertical axis shows the enrichment score. Different color curves represent distinct pathways

and HMGB1 also demonstrated differences (P-values < 0.05). The constructed PPI network, depicted in Fig. 2B, is based on these differential ICD-related genes. Each network node symbolizes the proteins produced by a single, protein-coding gene locus, with edges indicating protein-protein interactions. Different colors represent evidence validated from various databases or experimental sources.

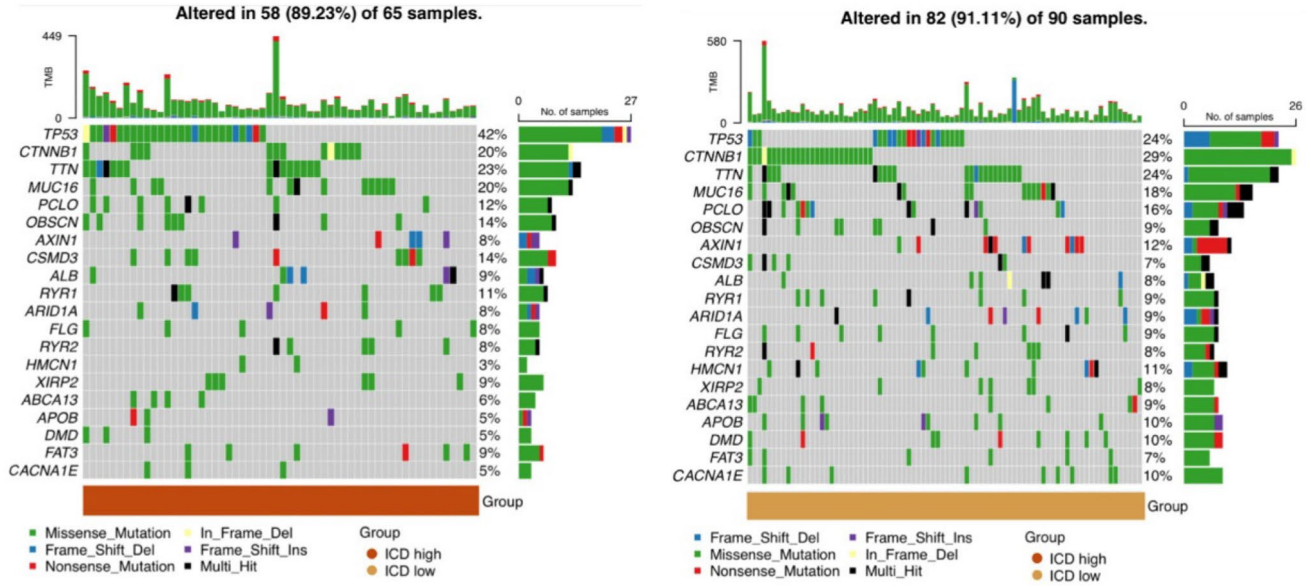

Fig. 6 Waterfall plot of gene mutations in ICD high and low expression groups. This plot displays gene mutations, with the horizontal axis representing samples and the vertical axis denoting genes. Different colors indicate various mutation types, allowing observation of each gene's mutation frequency

3.2 Identification of the ICD subgroups

Our objective was to achieve high correlation within subtypes and low correlation between them. Cluster analysis indicated that the highest consistency within groups occurred when K = 2, leading to the division of Asian HCC patients into two subtypes: C1 and C2 (Fig. 3A). Subsequent analysis of ICD-related gene expression revealed that subtype C1 corresponds to the high ICD expression group, while C2 aligns with the low ICD expression group (Fig. 3B).

3.3 Subgroup survival analysis

Survival analysis revealed that the ICD high expression group exhibited a lower survival rate compared to the ICD low expression group, with a statistically significant difference (P-value < 0.05) as shown in Fig. 4.

3.4 Subgroup difference analysis

Through differential analysis, we identified genes with varying expressions between the ICD high expression group and the ICD low expression group, as illustrated in Fig. 5A. GO enrichment analysis revealed that these differential genes were predominantly enriched in functions such as positive regulation of cell activation, external side of plasma membrane, and antigen binding, among others (Fig. 5B). Similarly, KEGG enrichment analysis showed an enrichment of differential genes in pathways like the PI3K–Akt signaling pathway, cytokine–cytokine receptor interaction, and regulation of the actin cytoskeleton, to name a few (Fig. 5C). Further, through GSEA, we explored potential signaling pathways differentiating the ICD high and low expression groups. Figure 5D, E suggest that pathways associated with the ICD high expression group might include cell adhesion molecules (CAMS), cytokine receptor interaction, etc., whereas the ICD low expression group may be linked with pathways such as butanoate metabolism, glycine serine and threonine metabolism, among others.

3.5 Subgroup mutation analysis

Mutation analysis indicated that genes such as TP53, MUC16, OBSCN, CSMD3, ALB, RYR1, XIRP2, and FAT3 exhibited higher mutation frequencies in the ICD high expression group compared to the ICD low expression group. Conversely,

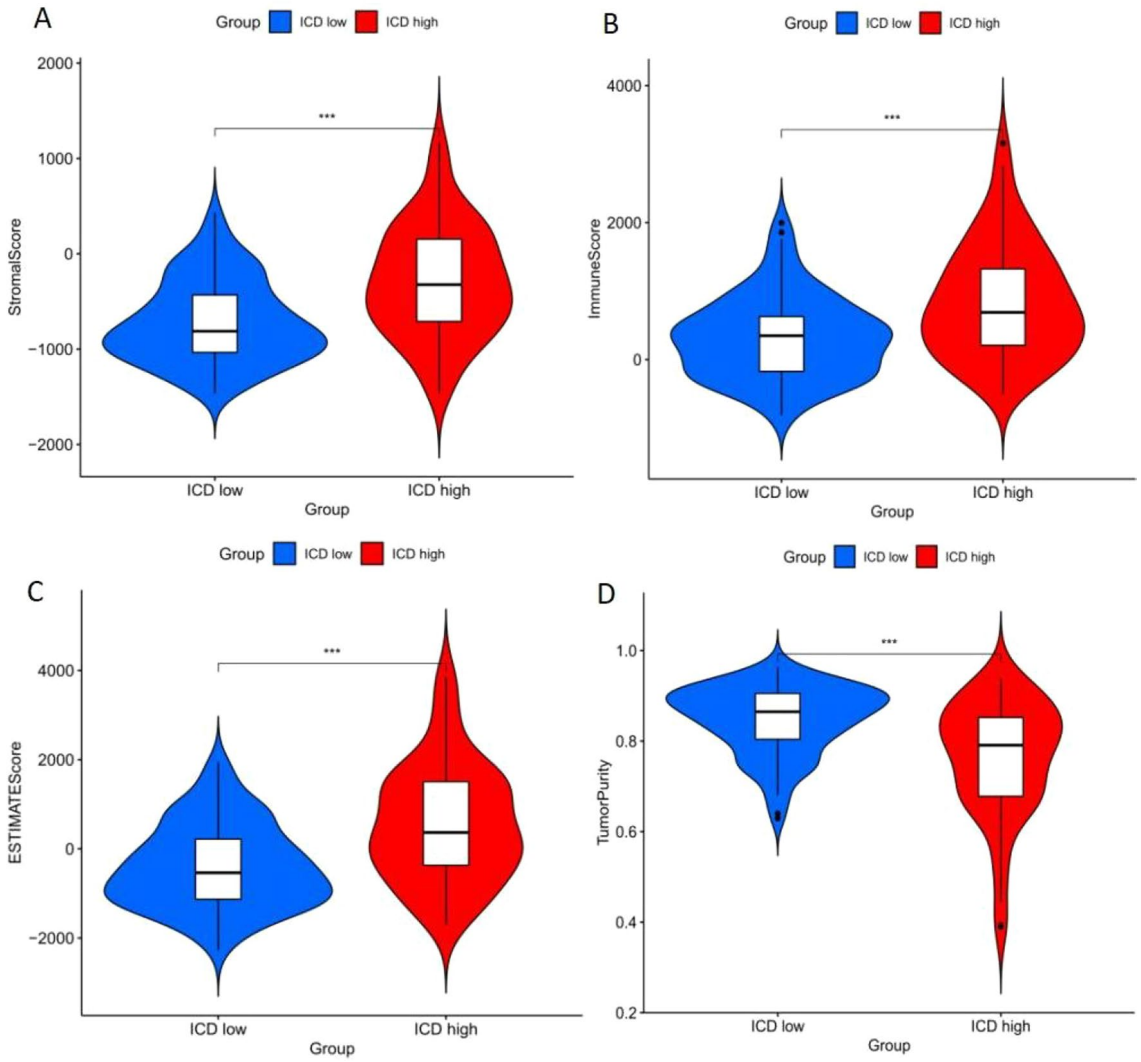

Fig. 7 Violin plot of tumor microenvironment in high and low ICD expression groups. **A** The stromal cell score; **B** the immune cell score; **C** the composite score; **D** tumor purity. The color blue represents the low ICD expression group, while red signifies the high ICD expression group. The vertical axis displays the tumor microenvironment score. ***Represents $p < 0.001$

genes including CTNNB1, TTN, PCLO, AXIN1, ARID1A, FLG, HMCN1, ABCA13, APOB, DMD, and CACNA1E showed higher mutation frequencies in the ICD low expression group. Notably, RYR2 maintained the same mutation frequency in both subgroups (Fig. 6).

3.6 Differential analysis of tumor microenvironment in subgroups

In terms of the tumor microenvironment, stromal and immune cells scored higher in the ICD high expression group compared to the ICD low expression group. Consequently, tumor purity was found to be greater in the ICD low expression group. This difference was statistically significant with a P-value less than 0.001 (Fig. 7).

3.7 Differential analysis of immune cells, HLA genes, and immune checkpoint-associated genes in subgroups

Through differential analysis, it was observed that only neutrophils showed significant variance between the ICD high and low expression groups. Their prevalence was higher in the ICD high expression group, with a P-value less

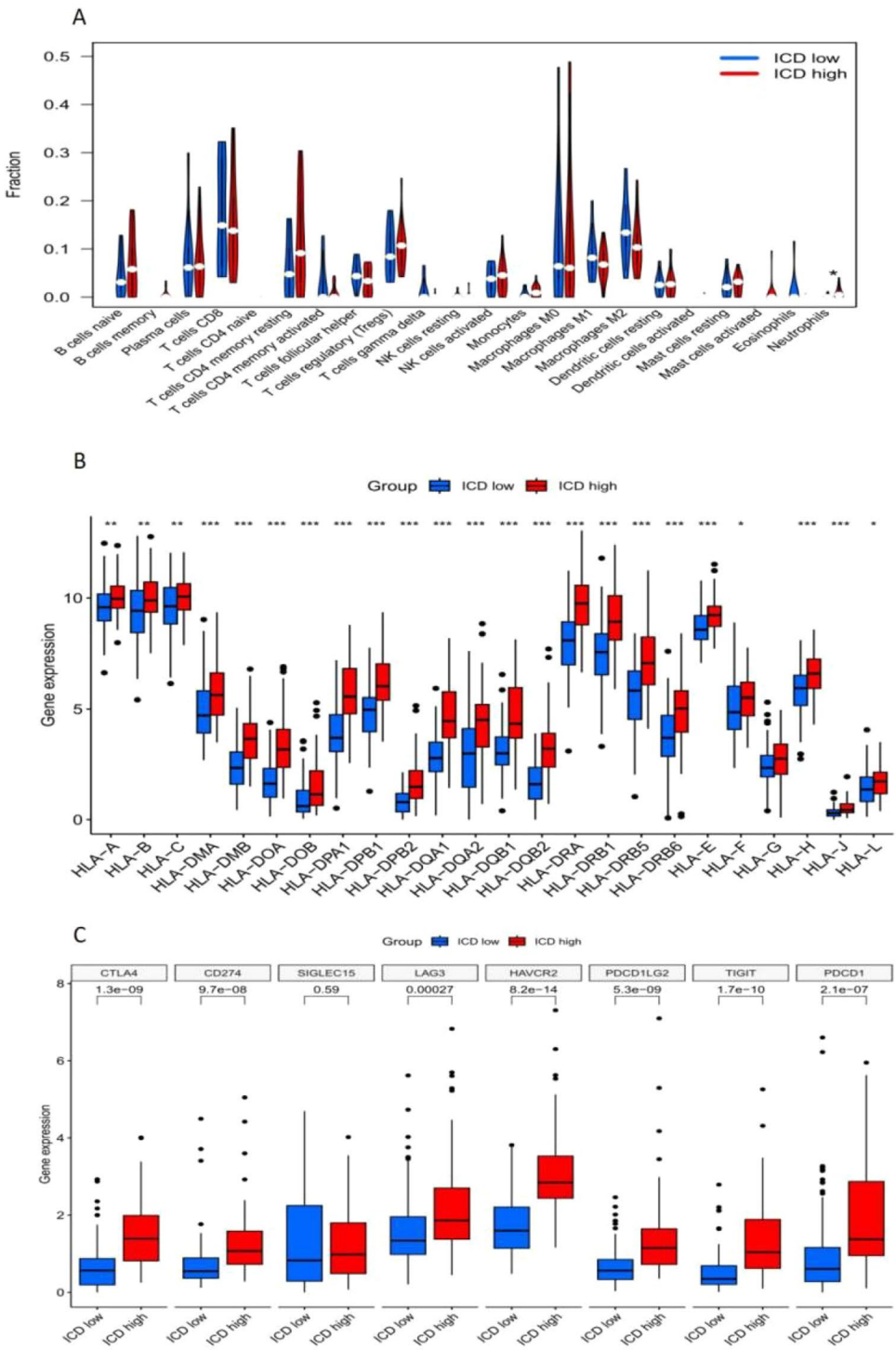

Fig. 8 Differential analysis of immune cells, HLA genes, and immune checkpoint-associated genes in ICD high and low expression groups. **A** Violin plot illustrating the content of immune cells in both ICD high and low expression groups. The horizontal axis labels the immune cell types, while the vertical axis quantifies their content. Blue denotes the ICD low expression group, and red indicates the ICD high expression group. An asterisk (*) signifies a difference in immune cell content between the high and low expression groups. **B** Box plot depicting HLA gene expression across the two groups. The horizontal axis shows HLA-related genes, and the vertical axis represents gene expression levels. Blue signifies the ICD low expression group, red the ICD high expression group. Significance levels are indicated: ***p value < 0.001, **p value < 0.01, *p value < 0.05. **C** Box plot of immune checkpoint-associated genes expression in the ICD high and low expression groups. The horizontal axis categorizes the sample groups, and the vertical axis measures gene expression. A p-value < 0.05 indicates significant differences

than 0.05, indicating statistical significance (Fig. 8A). The expression levels of certain HLA genes, as well as immune checkpoint-associated genes, were elevated in the ICD high expression group compared to the ICD low expression group. These differences were statistically significant, with p-values less than 0.05, as elaborated in Fig. 8B, C.

3.8 Construction of an ICD prognostic model

A 5-gene risk-score prognostic model (Fig. 9) was developed in the training group using Lasso–Cox analysis. The formula for the risk score was: risk score = $0.000521452 \times Exp_{BAX} + 0.008997493 \times Exp_{CASP8} + 0.001231 \times Exp_{HMGB1} + 0.001407455$

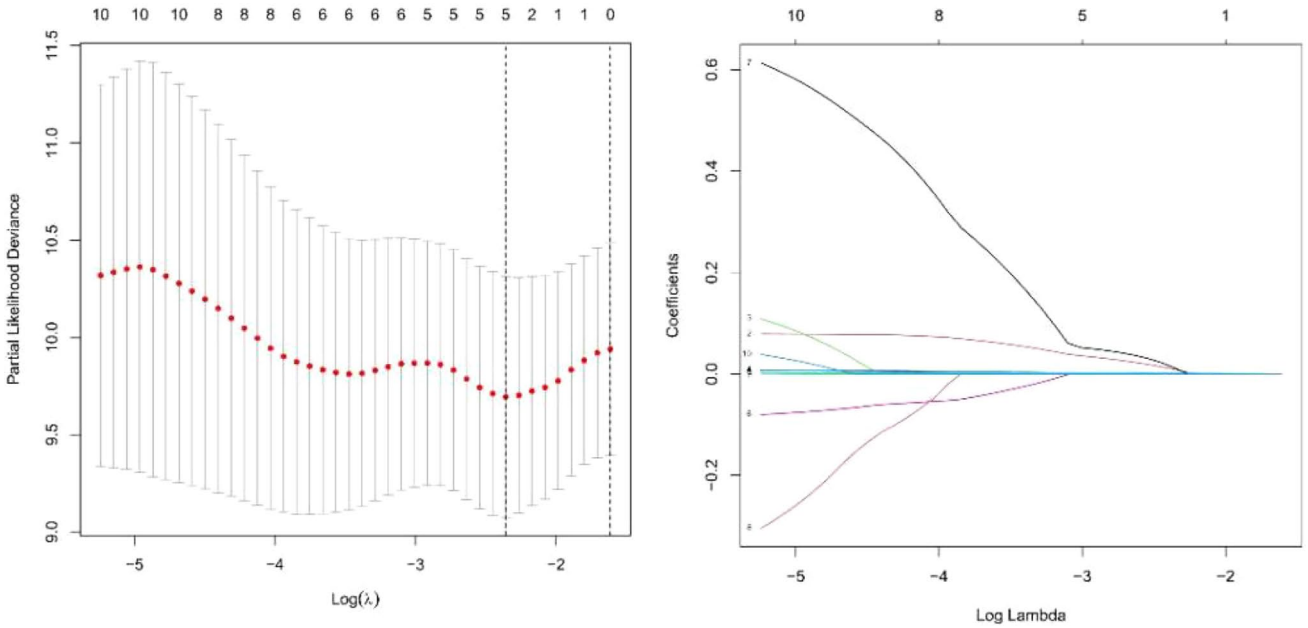

Fig. 9 Lasso–Cox analysis results in the training group. This figure displays the point of minimum cross-validation error, marked by a dotted line. The number of genes at this point corresponds to the number used in model construction

Table 2 The 5 ICD related genes involved in the construction of the risk score prognostic model

Gene	Coefficient
BAX	0.000521452
CASP8	0.008997493
HMGB1	0.001230689
HSP90AA1	0.001407455
IL6	0.011885139

$\times Exp_{HSP90AA1} + 0.011885139 \times Exp_{IL6}$ (Table 2). Subsequent validations of the model in the test group revealed, via K–M survival analysis, that the survival rate was higher in the low-risk group compared to the high-risk group in both training and test groups. The P-values were 0.008 in the training group and 0.023 in the test group, both below 0.05, thus statistically significant (Fig. 10A, B).

As depicted by the ROC curves in Fig. 10C, D, the AUC values were 0.783 for the training group and 0.655 for the test group, both exceeding 0.5, suggesting the model's moderate accuracy. Figure 10E, F illustrate the survival curves for the training and test groups, while Fig. 10G, H display the survival status, indicating a decrease in survival time and an increase in the number of deaths with escalating risk values in both groups.

3.9 Validation of the ICD prognostic model

Integrated data from both training and test groups, we conducted independent prognostic analysis and risk score-immune cell correlation analysis. The results indicated that the risk score prognostic model, based on ICD-related genes, could serve as an independent prognostic factor for the Asian HCC population (Fig. 11A, B). The risk score was found to be negatively correlated with M1 cells ($P = 0.033$) and γδ T cells ($P = 0.024$), both statistically significant correlations (Fig. 12).

The p-values for stage and risk score were below 0.05 in both univariate and multivariate Cox independent prognostic analyses, suggesting their validity as independent prognostic factors.

Fig. 10 Validation of the prognostic model. **A** K–M survival curves for the training group. **B** K–M survival curves for the testing group. The red curve represents the high-risk group, while the blue curve denotes the low-risk group. In both training and testing groups, the low-risk group exhibited significantly higher survival rates and longer survival times than the high-risk group ($p < 0.05$), indicating statistical significance. **C** ROC curve for the training group. **D** ROC curve for the testing group. The horizontal axis represents the false-positive rate, and the vertical axis the true-positive rate. The area under the curve reflects the model's accuracy. **E** Risk plot for the training group. **F** Risk plot for the testing group. Risk scores increase from left to right, with the median value indicated by a dotted line. The left green line represents low-risk patients, and the right red line indicates high-risk patients. **G** Survival time and status graph for the training group. **H** Survival time and status graph for the testing group. Red dots signify deceased patients, and green dots indicate living patients. As risk scores rise, survival time decreases and mortality rates incrementally increase

3.10 Clinical correlation analysis

We found that risk scores were related to age and pathological grade ($P = 0.009$, 0.010, respectively). Specifically, risk scores were higher in the ≤ 65y group than in the > 65y group (Fig. 13A). And compared to the grade 1–2 group, risk scores were lower in the grade 3–4 group (Fig. 13B). Although there was a tendency to show higher risk scores in the stage III–IV group than in the stage I–II group, this was not statistically significant ($P = 0.057$, Fig. 13C).

4 Discussion

The strong invasiveness of tumor lesions and the high mutation diversity within tumor cells enable these cells to circumvent the host's defense system, ultimately leading to tumor immune escape and uncontrolled proliferation. In such scenarios, tumor cells often exhibit low or even non-existent immunogenicity [15]. Immunogenicity is defined as the ability to elicit an immune response. Antigens play a crucial role in stimulating specific immune cells, aiding in their activation, proliferation, and differentiation, consequently producing substances related to immune effects, such as antibodies and related lymphocytes [19]. During tumor treatment, apoptosis in tumor cells is induced by various external stimuli. Moreover, tumor cells characterized by no or low immunogenicity are transformed into cells with normal immunogenicity. This transformation results in a form of regulated cell death (RCD) induced by specific stressors, which leads to antitumor immunity [13, 20]. This process is referred to as immunogenic cell death (ICD).

Transcriptome sequencing data, clinical characteristics, and gene mutation information for 161 Asian HCC patients were obtained from the TCGA database for analysis. The subtypes were categorized into ICD high and low expression groups based on ICD gene expression. The survival rate in the ICD high expression group was found to be higher than that in the ICD low expression group. It is worth noting that ICD-high and ICD-low groups are quite different in immune related genes; however, differential analysis in immunes showed no obvious differences except neutrophils. The immune system is highly complex and dynamic, with interactions between various cell types that can be difficult to capture in a single analysis. It is possible that while certain immune-related genes are differentially expressed, the overall functional impact on immune cell populations may be buffered by compensatory mechanisms or interactions between different cell types. The statistical power of the analysis to detect differences in immune cell populations may be limited by factors such as sample size, which could affect the ability to detect significant differences. We acknowledge the importance of sample size and its potential impact on the statistical significance of our findings. Moreover, Neutrophils have been reported in the literature to be associated with both promotional and suppressive roles in the tumor microenvironment, depending on the context. The observed difference in neutrophil populations could be a reflection of these complex interactions. Additionally, neutrophils are known to be one of the first responders to inflammation, and their presence could indicate a primed immune response that is not fully manifested in other immune cell subsets.

Through Lasso–Cox analysis, five ICD-relevant genes were identified, and a risk-score predictive model was established using BAX, CASP8, HMGB1, HSP90AA1, and IL6. Subsequent K–M survival analysis demonstrated that the survival rate of the low-risk group surpassed that of the high-risk group in both training and testing groups ($P < 0.05$). The Area Under the Curve (AUC) values for both groups exceeded 0.5, indicating a reasonable prognostic prediction capability. Additionally, it is suggested that these five genes included in the prediction model could serve as novel targets for ICD-related treatments in the future.

BCL2-associated X (BAX), a classical gene in apoptosis, is part of the Bcl-2 family's pro-apoptotic subgroup. The BAX protein, produced by this gene, is a pro-apoptotic factor that promotes cell death by forming homodimers, initiating

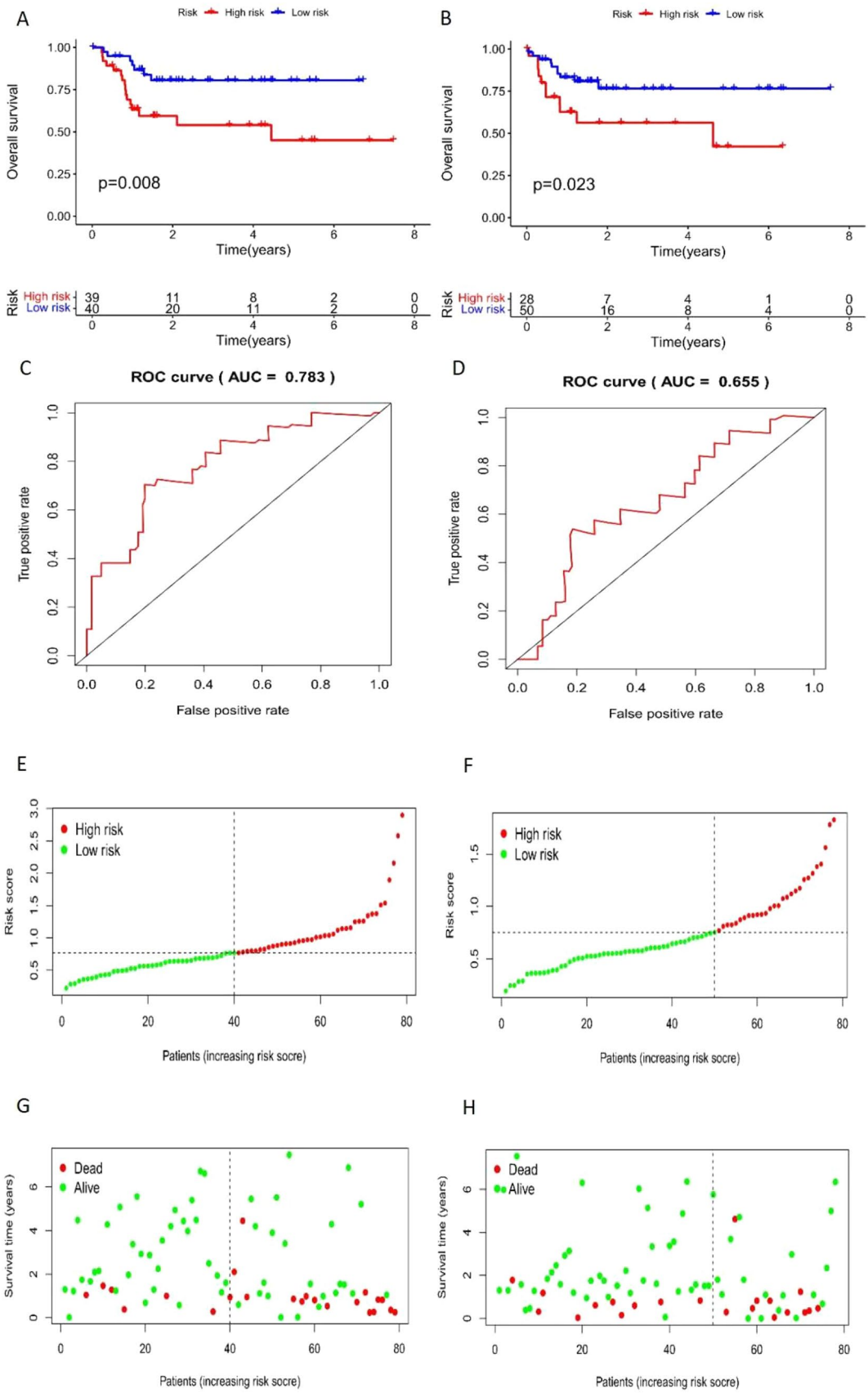
A
Risk High risk Low risk
Overall survival
p=0.008
Time(years)
Risk High risk 39 11 8 2 0
Low risk 40 20 11 2 0
B
Risk High risk Low risk
Overall survival
p=0.023
Time(years)
Risk High risk 28 7 4 1 0
Low risk 50 16 8 4 0
C
ROC curve (AUC = 0.783)
True positive rate
False positive rate
D
ROC curve (AUC = 0.655)
True positive rate
False positive rate
E
High risk
Low risk
Risk score
Patients (increasing risk socre)
F
High risk
Low risk
Risk score
Patients (increasing risk socre)
G
Dead
Alive
Survival time (years)
Patients (increasing risk socre)
H
Dead
Alive
Survival time (years)
Patients (increasing risk socre)

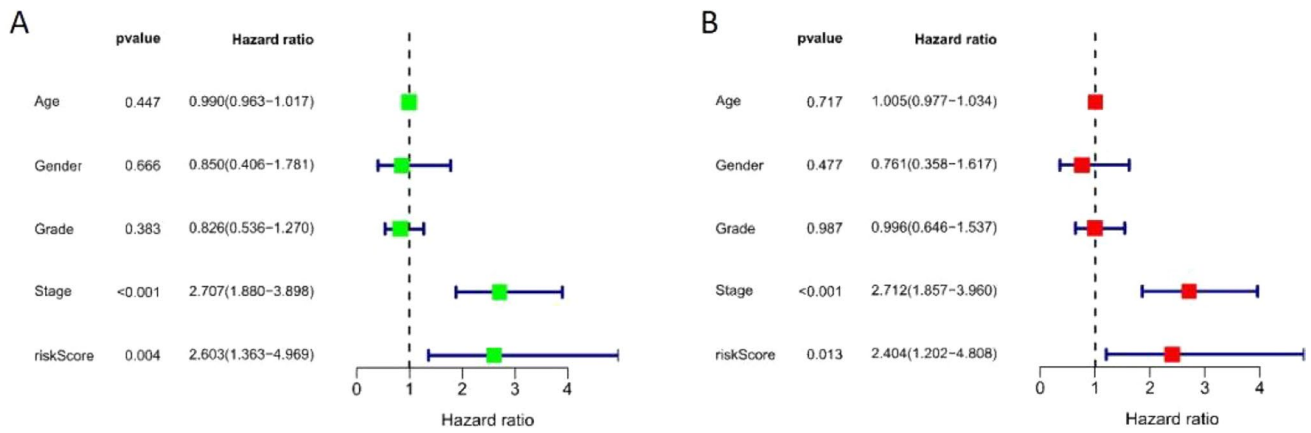

Fig. 11 Independent prognostic analysis. **A** Univariate cox independent prognostic analysis. **B** Multivariate cox independent prognostic analysis

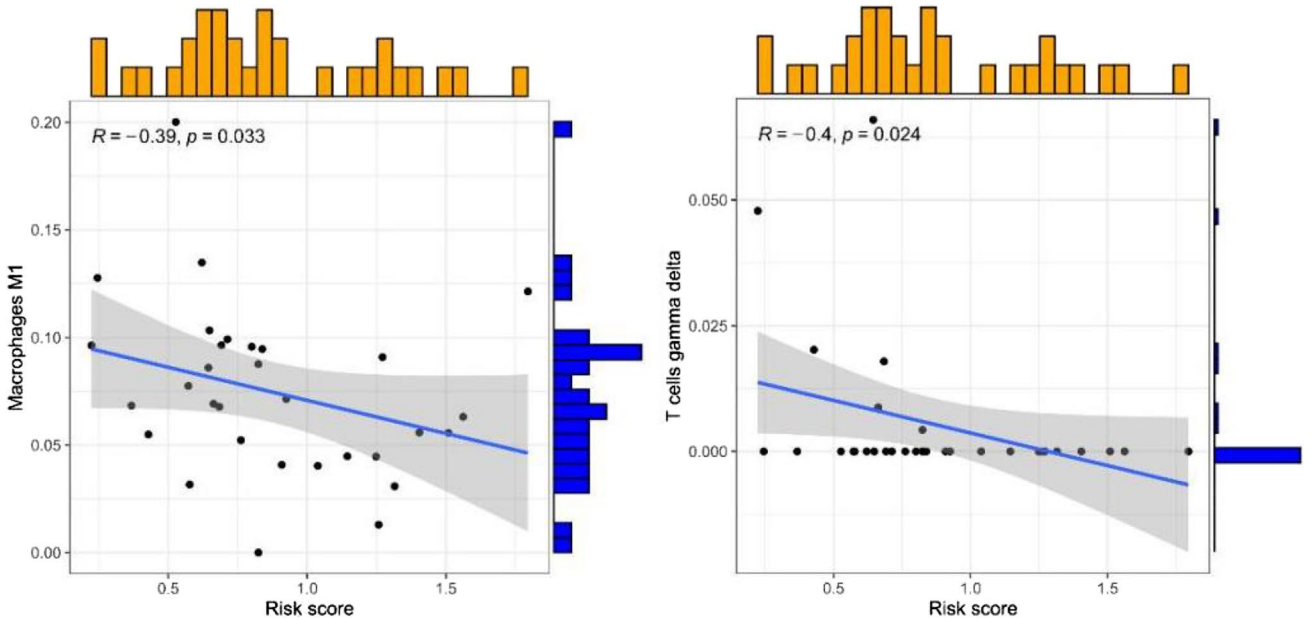

Fig. 12 Immune cell correlation

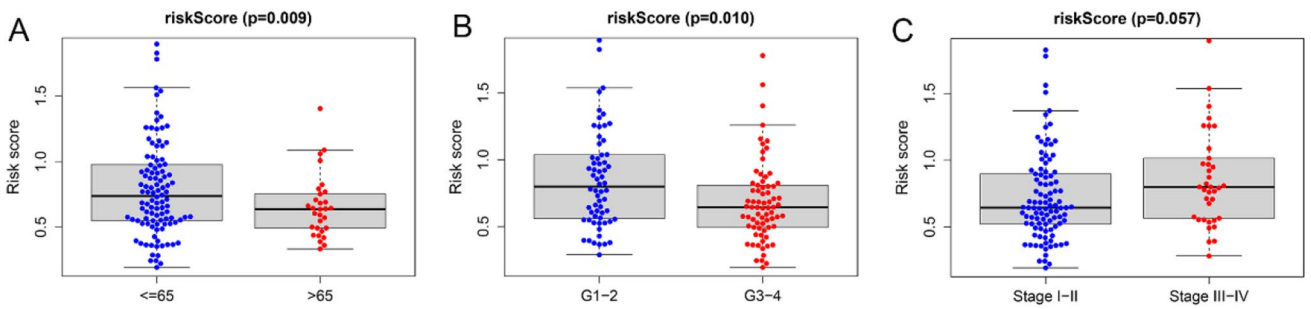

Fig. 13 Clinical correlation. **A** age; **B** grade; **C** stage

apoptosis, and inhibiting the anti-apoptotic functions of the B-cell lymphoma-2 gene (Bcl-2). The balance between BAX and Bcl-2 is a crucial factor in regulating apoptosis inhibition [21].

Caspase-8 (CASP8), a characteristic cysteine protease, is encoded by the CASP8 gene. Initially identified as an apoptotic caspase and an initiator of extrinsic cell death [22], recent research indicates that CASP8 is central to "PANoptosis", a comprehensive cell death mechanism intertwining pyroptosis, apoptosis, and necroptosis [23, 24].

High mobility group B1(HMGB1), is a nuclear non-histone chromatin-binding protein in the nucleus, mediating pro-inflammatory effects by interacting with toll-like receptor 4 (TLR4) on dendritic cells (DCs). It is released from dying cancer cells during immunogenic cell death (ICD) [13]. In this context, tumor cells release damage-associated molecular patterns (DAMPs), stimulating antitumor immune responses when undergoing ICD.

Heat shock protein 90α (Hsp90α), encoded by the heat shock protein 90 alpha family class A member 1 (HSP90AA1), facilitates oncogenesis by supporting various proteins associated with cancer progression [25]. Additionally, in prostate cancer, extracellular HSP90α has been observed to induce inflammation by activating transcription programs, including the production of pro-inflammatory cytokines like IL-6 and IL-8 [26].

The Interleukin (IL)−6 gene is co-expressed with various oncogenic genes [27]. IL-6, a pro-inflammatory cytokine with multifunctional effects, is produced and secreted by both immune and tumor cells. Dysregulation of IL-6 production and signaling has been linked to cancer and chronic inflammatory diseases [28].

Our study has several limitations. Firstly, all data were sourced from public databases, posing risks of insufficient sample size, missing data, and sample bias. Prospective clinical trials are necessary to validate the predictive ability of our findings. Secondly, the construction of the predictive model relied heavily on bioinformatics algorithms and databases, necessitating further experimental validation for accuracy. Thirdly, the association between the identified five genes and HCC remains unclear, requiring additional research for confirmation.

5 Conclusions

In conclusion, the prognostic prediction model for HCC patients developed in this study shows promise as a disease assessment tool. It could pave the way for personalized treatment approaches and targeted drug development in HCC.

Acknowledgements Not applicable.

Author contributions YW, YZ and YL conducted the computational analysis and authored the manuscript. XG and YY were instrumental in developing the prognostic risk-score model. ZF initiated the study and contributed to its design and coordination. QP and YZ were involved in drafting and revising the manuscript. All authors made significant contributions to the article and approved the final version.

Funding The current study was supported by the Second affiliated hospital of Soochow university pre-research project funding (SDFEYHT2225) and the Medical Applications of Nuclear Technology Project of the Second Affiliated Hospital of Soochow University (XKTJ-HRC20210013).

Data availability Data sources and handing of these data were described in Sect. 2. Further information is available from the corresponding author upon request. All data involved in this study are available in the public database. For further information, please contact the corresponding authors. Data is provided in a manuscript or supplementary information file where our data is available.

Declarations

Ethics approval and consent to participate Not applicable.

Consent for publication Not applicable.

Competing interests The authors declare no competing interests.

References

1. McGlynn KA, Petrick JL, El-Serag HB. Epidemiology of hepatocellular carcinoma. Hepatology. 2021;73(Suppl 1):4–13.
2. Rahib L, Smith BD, Aizenberg R, Rosenzweig AB, Fleshman JM, Matrisian LM. Projecting cancer incidence and deaths to 2030: the unexpected burden of thyroid, liver, and pancreas cancers in the United States. Cancer Res. 2014;74(11):2913–21.
3. Llovet JM, Kelley RK, Villanueva A, Singal AG, Pikarsky E, Roayaie S, Lencioni R, Koike K, Zucman-Rossi J, Finn RS. Hepatocellular carcinoma. Nat Rev Dis Prim. 2021;7(1):6.
4. Huang DQ, Mathurin P, Cortez-Pinto H, Loomba R. Global epidemiology of alcohol-associated cirrhosis and HCC: trends, projections and risk factors. Nat Rev Gastroenterol Hepatol. 2023;20(1):37–49.
5. Sia D, Jiao Y, Martinez-Quetglas I, Kuchuk O, Villacorta-Martin C, Castro de Moura M, Putra J, Camprecios G, Bassaganyas L, Akers N, Losic B, Waxman S, Thung SN, Mazzaferro V, Esteller M, Friedman SL, Schwartz M, Villanueva A, Llovet JM. Identification of an immune-specific class of hepatocellular carcinoma, based on molecular features. Gastroenterology. 2017;153(3):812–26.
6. Ruiz de Galarreta M, Bresnahan E, Molina-Sánchez P, Lindblad KE, Maier B, Sia D, Puigvehi M, Miguela V, Casanova-Acebes M, Dhainaut M, Villacorta-Martin C, Singhi AD, Moghe A, von Felden J, Tal Grinspan L, Wang S, Kamphorst AO, Monga SP, Brown BD, Villanueva A, Llovet JM, Merad M, Lujambio A. β-Catenin activation promotes immune escape and resistance to anti-PD-1 therapy in hepatocellular carcinoma. Cancer Discov. 2019;9(8):1124–41.
7. Krysko DV, Garg AD, Kaczmarek A, Krysko O, Agostinis P, Vandenabeele P. Immunogenic cell death and DAMPs in cancer therapy. Nat Rev Cancer. 2012;12(12):860–75.
8. DeNardo DG, Brennan DJ, Rexhepaj E, Ruffell B, Shiao SL, Madden SF, Gallagher WM, Wadhwani N, Keil SD, Junaid SA, Rugo HS, Hwang ES, Jirström K, West BL, Coussens LM. Leukocyte complexity predicts breast cancer survival and functionally regulates response to chemotherapy. Cancer Discov. 2011;1(1):54–67.
9. Denkert C, Loibl S, Noske A, Roller M, Müller BM, Komor M, Budczies J, Darb-Esfahani S, Kronenwett R, Hanusch C, von Törne C, Weichert W, Engels K, Solbach C, Schrader I, Dietel M, von Minckwitz G. Tumor-associated lymphocytes as an independent predictor of response to neoadjuvant chemotherapy in breast cancer. J Clin Oncol. 2010;28(1):105–13.
10. Halama N, Michel S, Kloor M, Zoernig I, Benner A, Spille A, Pommerencke T, von Knebel DM, Folprecht G, Luber B, Feyen N, Martens UM, Beckhove P, Gnjatic S, Schirmacher P, Herpel E, Weitz J, Grabe N, Jaeger D. Localization and density of immune cells in the invasive margin of human colorectal cancer liver metastases are prognostic for response to chemotherapy. Cancer Res. 2011;71(17):5670–7.
11. Zhu H, Shan Y, Ge K, Lu J, Kong W, Jia C. Oxaliplatin induces immunogenic cell death in hepatocellular carcinoma cells and synergizes with immune checkpoint blockade therapy. Cell Oncol. 2020;43(6):1203–14.
12. Yu Z, Guo J, Hu M, Gao Y, Huang L. Icaritin exacerbates mitophagy and synergizes with doxorubicin to induce immunogenic cell death in hepatocellular carcinoma. ACS Nano. 2020;14(4):4816–28.
13. Ahmed A, Tait SWG. Targeting immunogenic cell death in cancer. Mol Oncol. 2020;14(12):2994–3006.
14. Garg AD, De Ruysscher D, Agostinis P. Immunological metagene signatures derived from immunogenic cancer cell death associate with improved survival of patients with lung, breast or ovarian malignancies: a large-scale meta-analysis. Oncoimmunology. 2016;5(2):e1069938.
15. Kroemer G, Galassi C, Zitvogel L, Galluzzi L. Immunogenic cell stress and death. Nat Immunol. 2022;23(4):487–500.
16. Galluzzi L, Vitale I, Warren S, Adjemian S, Agostinis P, Martinez AB, Chan TA, Coukos G, Demaria S, Deutsch E, Draganov D, Edelson RL, Formenti SC, Fucikova J, Gabriele L, Gaipl US, Gameiro SR, Garg AD, Golden E, Han J, Harrington KJ, Hemminki A, Hodge JW, Hossain DMS, Illidge T, Karin M, Kaufman HL, Kepp O, Kroemer G, Lasarte JJ, Loi S, Lotze MT, Manic G, Merghoub T, Melcher AA, Mossman KL, Prosper F, Rekdal Ø, Rescigno M, Riganti C, Sistigu A, Smyth MJ, Spisek R, Stagg J, Strauss BE, Tang D, Tatsuno K, van Gool SW, Vandenabeele P, Yamazaki T, Zamarin D, Zitvogel L, Cesano A, Marincola FM. Consensus guidelines for the definition, detection and interpretation of immunogenic cell death. J Immunother Cancer. 2020;8(1):e000337.
17. Ping L, He Y, Gao Y, Wang X, Huang C, Bai B, Huang H. Immunogenic cell death (ICD)-related gene signature could predict the prognosis of patients with diffuse large B-cell lymphoma. J Pers Med. 2022;12(11):1840.
18. Wang Z, Liu J, Wang Y, Guo H, Li F, Cao Y, Zhao L, Chen H. Identification of key biomarkers associated with immunogenic cell death and their regulatory mechanisms in severe acute pancreatitis based on WGCNA and machine learning. Int J Mol Sci. 2023;24(3):3033.
19. Blankenstein T, Coulie PG, Gilboa E, Jaffee EM. The determinants of tumour immunogenicity. Nat Rev Cancer. 2012;12(4):307–13.
20. Zhu M, Yang M, Zhang J, Yin Y, Fan X, Zhang Y, Qin S, Zhang H, Yu F. Immunogenic cell death induction by Ionizing radiation. Front Immunol. 2021;12:705361.
21. He G, Li LI, Guan E, Chen J, Qin YI, Xie Y. Fentanyl inhibits the progression of human gastric carcinoma MGC-803 cells by modulating NF-κB-dependent gene expression in vivo. Oncol Lett. 2016;12(1):563–71.
22. Han JH, Park J, Kang TB, Lee KH. Regulation of Caspase-8 activity at the crossroads of pro-inflammation and anti-inflammation. Int J Mol Sci. 2021;22(7):3318.
23. Jiang M, Qi L, Li L, Wu Y, Song D, Li Y. Caspase-8: a key protein of cross-talk signal way in PANoptosis in cancer. Int J Cancer. 2021;149(7):1408–20.
24. Newton K, Wickliffe KE, Maltzman A, Dugger DL, Reja R, Zhang Y, Roose-Girma M, Modrusan Z, Sagolla MS, Webster JD, Dixit VM. Activity of caspase-8 determines plasticity between cell death pathways. Nature. 2019;575(7784):679–82.
25. Zuehlke AD, Beebe K, Neckers L, Prince T. Regulation and function of the human HSP90AA1 gene. Gene. 2015;570(1):8–16.
26. Bohonowych JE, Hance MW, Nolan KD, Defee M, Parsons CH, Isaacs JS. Extracellular Hsp90 mediates an NF-κB dependent inflammatory stromal program: implications for the prostate tumor microenvironment. Prostate. 2014;74(4):395–407.
27. Shen S, Kong J, Qiu Y, Yang X, Wang W, Yan L. Identification of core genes and outcomes in hepatocellular carcinoma by bioinformatics analysis. J Cell Biochem. 2019;120(6):10069–81.
28. Ataie-Kachoie P, Pourgholami MH, Morris DL. Inhibition of the IL-6 signaling pathway: a strategy to combat chronic inflammatory diseases and cancer. Cytokine Growth Factor Rev. 2013;24(2):163–73.